
Compelling ReLU Network Initialization and Training to Leverage Exponential Scaling with Depth

Max Milkert*

max.milkert@vanderbilt.edu

David Hyde*

david.hyde.1@vanderbilt.edu

Forrest Laine*

forrest.laine@vanderbilt.edu

Abstract

A neural network with ReLU activations may be viewed as a composition of piecewise linear functions. For such networks, the number of distinct linear regions expressed over the input domain has the potential to scale exponentially with depth, but it is not expected to do so when the initial parameters are chosen randomly. This poor scaling can necessitate the use of overly large models to approximate even simple functions. To address this issue, we introduce a novel training strategy: we first reparameterize the network weights in a manner that forces the network to display a number of activation patterns exponential in depth. Training first on our derived parameters provides an initial solution that can later be refined by directly updating the underlying model weights. This approach allows us to learn approximations of convex, one-dimensional functions that are several orders of magnitude more accurate than their randomly initialized counterparts.

1 Introduction

Beyond complementary advances in areas like hardware, storage, and networking, the success of neural networks is primarily due to their ability to efficiently capture and represent nonlinear functions [Gibou et al., 2019]. In a neural network, the goal of an activation function is to introduce nonlinearity between the network’s layers so that the network does not simplify to a single linear function. The rectified linear unit (ReLU) has a unique interpretation in this regard. Since it either deactivates a neuron or acts as an identity, the resulting transformation on each individual input remains linear. However, each possible configuration of active and inactive neurons can produce a unique linear transformation over a particular region of input space. The number of these activation patterns and their corresponding linear regions provides a way to measure the expressivity of a ReLU network, and can theoretically scale exponentially with the depth of the network². Hence deep architectures may outperform shallow ones.

Surprisingly, though, a sophisticated theory of how to best encode functions into ReLU networks is lacking, and in practice, adding depth is often observed to help less than one might expect from this exponential intuition. Lacking more advanced theory, practitioners typically use random parameter initialization and gradient descent, the drawbacks of which often lead to extremely inefficient solutions. Hanin and Rolnick [2019] show a rather disappointing bound pertaining to randomly initialized networks: they prove that the average number of linear regions formed upon initialization is entirely independent of the configuration of the neurons, so depth is not properly utilized. They

*Department of Computer Science, Vanderbilt University, Nashville TN 37325

²The reader is referred to Chmielewski-Anders [2020] for definitions of linear regions, activation patterns, and activation regions.

observed that gradient descent has a difficult time creating new activation regions and that their bounds approximately held after training. As we will discuss later, the number of linear regions is not actually a model property that gradient descent can directly optimize. Gradient descent is also prone to redundancy; Frankle and Carbin [2019] show how up to 90% of neurons may ultimately be eliminated from a network without significantly degrading accuracy.

The present work aims to begin eliminating these inefficiencies, starting in a simple one-dimensional setting. Drawing inspiration from existing theoretical ReLU constructions, our novel contributions include a special reparameterization of a ReLU network that forces it to maintain an exponential number of activation patterns over the input domain. We then demonstrate a novel pretraining strategy, which trains these derived parameters before manipulating the underlying matrix weights. This allows the network to discover solutions that are more accurate and unlikely to be found otherwise. Our technique directly rectifies the issues raised by Hanin and Rolnick [2019]. Firstly, we initialize immediately with an exponential number of linear regions, which would not be expected to happen otherwise. Secondly, we are not reliant on gradient descent to “discover” new regions; we only need to maintain the existing ones, which is already guaranteed by the reparameterization during the pretraining stage. Additionally, this pretraining step can avoid areas of the loss landscape where unassisted gradient descent might make short-sighted optimizations that eliminate activation regions. Our results demonstrate that minimizing the reliance of network training on unassisted gradient descent can reliably produce error values orders of magnitude lower than a traditionally-trained network of equal size. Although the preliminary results in this theoretical study pertain to one-dimensional convex functions, the paper concludes with our views on extending these theoretical exponential benefits for ReLU networks to arbitrary smooth functions with arbitrary dimensionality, which would have significant practical utility.

2 Related Work

This work is primarily concerned with a novel training methodology, but it also possesses a significant approximation theoretic component. Our work can be viewed as a first step towards generalizing the approximation to x^2 we review in this section. The reparameterization we employ modifies this method to become trainable in order to represent other convex one-dimensional functions, and then converts that result back into a matrix representation.

2.1 Related Work in Approximation

Infinitely wide neural networks are known to be universal function approximators, even with only one hidden layer [Hornik et al., 1989, Cybenko, 1989]. Infinitely deep networks of fixed width are universal approximators as well [Lu et al., 2017, Hanin, 2019]. In finite cases, the trade-off between width and depth is often studied in assessing a network’s ability to approximate (learn) a function.

Notably, there exist functions that can be represented with a sub-exponential number of neurons in a *deep* architecture, yet which require an exponential number of neurons in a *wide and shallow* architecture. For example, Telgarsky [2015] shows that deep neural networks with ReLU activations on a one-dimensional input are able to generate symmetric triangle waves with an exponential number of linear segments (shown in Figure 1 as the ReLU network $T(x)$). This network functions as follows: each layer takes a one-dimensional input on $[0, 1]$, and outputs a one-dimensional signal also on $[0, 1]$. The function they produce in isolation is a single symmetric triangle. Together in a network, each layer inputs its output to the next, performing function composition. Since each layer converts lines from 0 to 1 into triangles, it doubles the number of linear segments in its input signal, exponentially scaling with depth.

The novel reparameterization strategy contributed by the present work aims to extend this idea, compelling ReLU networks to compose rapidly oscillating triangular signals. The key insight is that instead of expressing each layer by its weights, we can train the location on $(0, 1)$ of a triangular function’s peak and then set that layer’s weights accordingly. Composing the layers together will create a variety of dilated triangular waveforms that the network can use in its approximations. We emphasize that while the Telgarsky [2015] approximation uses fixed symmetric triangles and is not trainable, a key insight of our work is to instead leverage non-symmetric triangles, which yields trainable parameters (one per triangle).

Nonetheless, with only symmetric triangle waves, Yarotsky [2017] and Liang and Srikant [2016] demonstrate the ability to construct $y = x^2$ on $[0, 1]$ with exponential accuracy. To produce their approximation, one begins with $f_0(x) = x$, then computes $f_1(x) = f_0(x) - T(x)/4$, $f_2(x) = f_1(x) - T(T(x))/16$, $f_3(x) = f_2(x) - T(T(T(x)))/64$, and so forth, as pictured in Figure 1. As these successive approximations are computed, Figure 1 plots their convergence to x^2 , as well as the convergence of the derivatives. We note that these prior papers explicitly focus on approximating x^2 using symmetric triangle waves, unlike the present work, which is more general (although those papers leverage their x^2 approximation to also indirectly build approximations of other functions).

The techniques of Yarotsky [2017] and Liang and Srikant [2016] seem to touch on something fundamental regarding how ReLU networks can approximate functions: even though individual neuron outputs may be jagged (e.g., Figure 1, top row), an appropriate infinite sum of them (e.g., $f_\infty(x)$) may still be differentiable. Moreover, the derivative of the approximation produced by this technique also converges to the true solution $y = 2x$ in the limit. Therefore, inspired by the exponential accuracy of this technique, we place a particular emphasis on investigating the relative importance of differentiability throughout the paper. We will argue with numerical evidence that enforcing convergence of the derivative can reduce the number of local minima during training.

One of the appealing properties of neural networks is that they are highly modular. The x^2 approximation is used by other theoretical works as a building block to guarantee exponential convergence rates in more complex systems. One possible use case is to construct a multiplication gate. Perekrestenko et al. [2018] does so via the identity $(x + y)^2 = x^2 + y^2 + 2xy$. The squared terms can all be moved to one side, expressing the product as a linear combination of squared terms. They then further assemble these multiplication gates into an interpolating polynomial, which can have an exponentially decreasing error when the interpolation points are chosen to be the Chebyshev nodes. Polynomial interpolation does not scale well into high dimensions, so this and papers with similar approaches will usually come with restrictions that limit function complexity: Wang et al. [2018] requires low input dimension, Montanelli et al. [2020] uses band limiting, and Chen et al. [2019] approximates low dimensional manifolds. In light of these prior papers, the present work revisits the x^2 approximation, seeking a generalization that can avoid the limitations of these works. Replacing x^2 with a more flexible class of functions may produce a suitable building block for techniques that can bypass polynomial interpolation.

Lastly, other works focus on showing how ReLU networks can encode and subsequently surpass traditional approximation methods [Lu et al., 2021, Daubechies et al., 2022]. Interestingly, certain fundamental themes from above like composition, triangles, or squaring are still present. One other interesting comparison of the present work is to Ivanova and Kubat [1995], which uses decision trees as a means to initialize neural networks. It is a sigmoid/classification analogy to this work, but rather than an attempting to improve neural networks with decision trees, it is an attempt to improve decision trees with neural networks.

2.2 Related Work in Initialization

Our work seeks to improve network initialization by making use of explicit theoretical constructs. This stands in sharp contrast the current standard approach, which treats neurons homogeneously. Two popular initialization methods implemented in PyTorch are the Kaiming [He et al., 2015] and Xavier initialization [Glorot and Bengio, 2010]. They use weight values that are sampled from distributions defined by the input and output dimension of each layer. Aside from sub-optimal approximation power associated with random weights, a common issue is that an entire ReLU network can collapse into outputting a constant value at initialization. This is referred to as the dying ReLU phenomenon [Qi et al., 2024, Nag et al., 2023]. It occurs when the initial weights and biases cause every neuron in a particular layer to output a negative value. The ReLU activation then sets the output of that layer to 0, blocking any gradient updates. Worryingly, as depth goes to infinity, the dying ReLU phenomenon becomes increasingly likely [Lu et al., 2020]. Several papers propose solutions: Shin and Karniadakis [2020] use a data-dependent initialization, while Singh and Sreejith [2021] introduce an alternate weight distribution called RAAI that can reduce the likelihood of the issue and increase training speed. We observed during our experiments that RAAI greatly reduces, but does not eliminate the likelihood of dying ReLU. Our approach enforces a specific network structure that does not collapse in this manner.

3 Compositional Networks

We begin by discussing how to deliberately architect the weights of a 4-neuron-wide, depth d ReLU network to induce a number of linear segments exponential in d . Throughout the paper, we refer to these as *compositional networks*. First we will introduce their mathematical form, and then we will discuss how to encode them as ReLU networks.

We define a triangle function as

$$T_i(x) = \begin{cases} \frac{x}{a_i} & 0 \leq x \leq a_i \\ 1 - \frac{x-a_i}{1-a_i} & a_i \leq x \leq 1 \end{cases}$$

where $0 \leq a_i \leq 1$. This produces a triangular shape with a peak at $x = a_i$ and with both endpoints at $y = 0$. Each layer in a compositional network in isolation would compute these if directly fed the input signal. $T_i(x)$'s derivatives are the piecewise linear functions:

$$T'_i(x) = \begin{cases} \frac{1}{a_i} & 0 < x < a_i \\ \frac{1}{1-a_i} & a_i < x < 1 \end{cases} \quad (1)$$

In a compositional network, the layers feed into each other. This composes triangle functions into triangle waves:

$$W_i(x) = \bigcirc_{j=0}^i T_j(x) = T_i(T_{i-1}(\dots T_0(x))) \quad (2)$$

The output of a compositional network will be a weighted sum over the triangle waves formed at each layer. Assuming the network to be infinitely deep, we have

$$F(x) = \sum_{i=0}^{\infty} s_i W_i(x) \quad (3)$$

where s_i are scaling coefficients on each of the composed triangular waveforms W_i .

To encode these functions into a ReLU network, we begin with triangle functions. This is the subnetwork on the right in Figure 2. Its maximum output is 1 at the peak location $a \in (0, 1)$. Neuron t_1 simply preserves the input signal. Meanwhile, t_2 is negatively biased, deactivating it for inputs less than a . Subtracting t_2 from t_1 changes the slope at the point where t_2 begins outputting a nonzero signal. The weight $-1/(a - a^2) = -(1/a + 1/(1-a))$ is picked to completely negate t_1 's positive influence, and then produce a negative slope. When these components are combined into a deep network, the individual triangles they form will be composed with those earlier in the network, but the two neurons will still behave analogously. Considering the output waveform of t_1 and t_2 neurons over the entire input domain $[0, 1]$ and at arbitrary depth, we have that t_1 neurons are always active, outputting complete triangle waves. In contrast, t_2 neurons are deactivated for small inputs, so they output an alternating sequence of triangles and inactive regions, which can be seen in Figure 3.

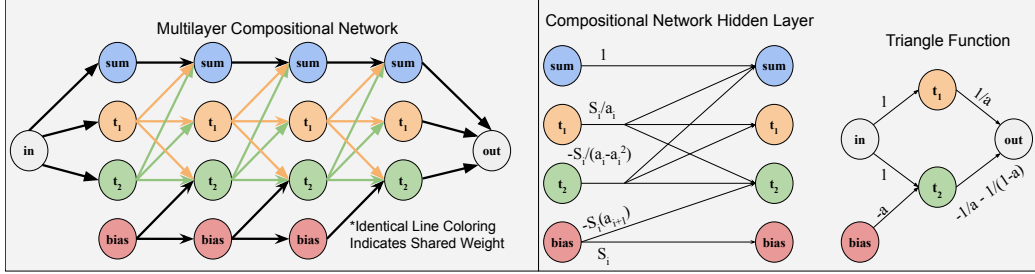


Figure 2: The rightmost diagram is a network representation of a triangle function. The middle shows that triangle function as a hidden layer of a compositional network. The one-dimensional input and output of a triangle function is instead converted into shared weights within the layers. A full compositional network is assembled on the left.

Naively using the output of one triangle generator (from Figure 2) as input to the next would form a $1 \times 2 \times 1 \times 2 \times 1 \dots$ shape, but this is unnecessarily deep. We can replicate the one-dimensional function composition in the hidden layers on the left side of Figure 2 by using weight sharing instead. Any outgoing weight from t_1 or t_2 is shared; every neuron taking in a triangle wave as input does so by combining t_1 and t_2 in the same proportion. In this way, we can avoid having to use the extra intermediate neurons. Notice in Figure 3 how the waves output by t_1 and t_2 neurons always have identical slopes in regions where both neurons are active.

There are two other neurons in the compositional network’s layers. The accumulation neuron (marked as “sum” in Figure 2) acts similarly to a skip connection, maintaining a weighted sum of all previous triangle waves through each layer. If this were naively implemented, it would multiply the t_1 and t_2 weights by the sum coefficients. Based on the derivations in the appendix, these coefficients will be exponentially decaying, so learning these weights directly may cause conditioning issues. Instead, all weights in each layer are multiplied by the ratios between successive scaling coefficients, so that the outputs of t_1 and t_2 neurons decay in amplitude in each layer. A conventional bias will have no connections to prior layers, so it will be unable to adjust to the rescaling neuron outputs without having to learn exponentially small values. Therefore, a fourth neuron is configured to output a constant signal, so the weight other neurons place on this output can replace their bias. The bias neuron will connect to the previous layer’s bias neuron so that the constant signal can scale down gradually with each layer.

3.1 Differentiable Model Output

Given the rapid oscillations of the triangle waves formed at each layer, the resulting output of the network will appear jagged with most choices of scaling parameters. This can lead to the network settling into overfit local minima, in which the data points might lie along the curve, but the curve is not predictive of the areas in between due to rapid oscillation. Our main mathematical result addresses this issue by forcing differentiability of the network output. It turns out that for this class of functions, the peak locations of the triangle waves uniquely determine the scales with which to sum them.

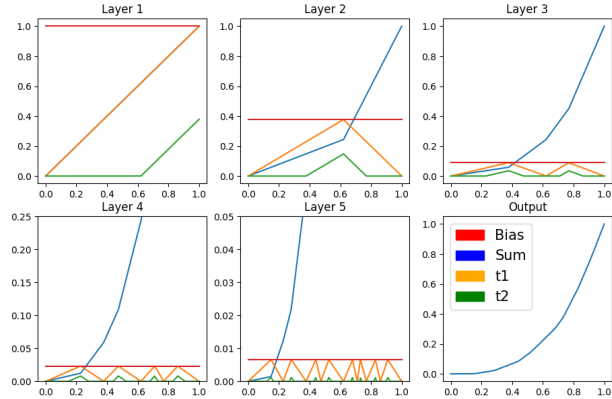


Figure 3: Each colored line shows the output signal of a neuron with respect to the input to the network. Colors match the corresponding neurons in Figure 2.

Theorem 3.1. $F'(x)$ is defined on $[0, 1]$ only if the scaling coefficients s_i are selected based on the triangle peaks a_i according to:

$$s_{i+1} = s_i(1 - a_{i+1})a_{i+2} \quad (4)$$

4 Experiments

The goal of deep learning is to train a network to approximate a (generally unknown) nonlinear function. Accordingly, in this section, we implement our method to learn several convex one-dimensional curves. These nonlinear functions are known—so that we can measure error—and we remark on more difficult functions in Sections 5 and 6. The aim of these experiments is twofold: (1) we would like to determine how to learn the most effective function representations possible, and (2) to explore how the utilization of an increased number of linear regions can affect a network’s ability to capture underlying nonlinearity in its training data. To demonstrate that our networks can learn function representations that better utilize depth, we benchmark against PyTorch’s default settings (`nn.linear()` uses Kaiming initialization), as well as the RAAI distribution from Singh and Sreejith [2021], and produce errors that are *orders of magnitude lower than both*. For our experimental networks, we use a common set of initialization points where the triangle peaks and scaling parameters are chosen according to our main theorem (Equation (4)). We compare the effect of reparameterized pretraining against skipping immediately to standard gradient descent. We also compare training the scaling parameters freely during pretraining, instead of choosing them to achieve differentiability. The intent of both comparisons is see if pretraining and differentiability constraints facilitate smoother navigation of the loss landscape and avoidance of local minima. Lastly, we conduct a second round of tests to determine if pretrained networks display an enhanced predictive capacity on unseen data points, as might be expected if they can leverage greater nonlinearity in their outputs.

4.1 Experimental Setup

All models are trained using Adam [Kingma and Ba, 2017] as the optimizer with a learning rate of 0.0001 for 1,000 epochs to ensure convergence. Each network is four neurons wide with five hidden layers, along with a one-dimensional input and output. The loss function used is the mean squared error, and the average and minimum loss are recorded for 30 models of each type. The networks unique to this paper share a common set of starting locations, so that the effects of each training regimen are directly comparable. As in related papers [Perekrestenko et al., 2018, Daubechies et al., 2022], we restrict our attention to one-dimensional examples, which are sufficient to demonstrate our proposed theory and methodology. The four curves we approximate are x^3 , x^{11} , $\tanh(3x)$, and a quarter period of a sine wave. The curves are chosen to capture a variety of convex one-dimensional functions. To approximate the sine and the hyperbolic tangent, the triangle waves are added to the line $y = x$. For the other approximations, the waves are subtracted. This requires the first scaling factor to be $a_0 * a_1$ instead of $(1 - a_0) * a_1$. The first set of data is 500 evenly spaced points on the interval $[0, 1]$ for each of the curves. This is chosen to be very dense deliberately, to try to evoke the most accurate representations from each network. We determine from these tests that pretraining with differentiability enforced produces the best results, so we compare it to standard networks in our second set of experiments. We use a second set of data consisting of only 10 points, with a test set of 10 points spaced in between so as to be as far away from learned data as possible. The goal of this set of experiments is to compare the predictive capacities of the networks on unseen data.

4.2 Numerical Results

Our first set of results are shown in Tables 1 and 2, wherein we observe several important trends. First, the worst performing networks are those that rely on purely randomized initializations. Even the networks that forgo pretraining benefit from initializing with many activation regions. When pretraining constraints are used, they are able to steer gradient descent to the best solutions, resulting in reductions in minimum error of three orders of magnitude over default networks.

Pretraining with differentiability enforced also closes the gap between the minimum and mean errors compared to other setups. This indicates that these loss landscapes are indeed the most reliable to traverse. Even in our noiseless setting, we find that it is still possible to settle into local minima where the function fits only a small subset of the data points and fails to accurately represent the target curve

Table 1: Minimum and mean (30 samples) MSE error approximating $y = x^3$ and x^{11} .

Training Type	Min x^3	Min x^{11}	Mean x^3	Mean x^{11}
Default Network	2.11×10^{-5}	2.19×10^{-5}	7.20×10^{-2}	2.82×10^{-2}
RAAI Distribution	2.14×10^{-5}	4.40×10^{-5}	3.97×10^{-2}	4.12×10^{-2}
Pretraining Skipped	7.63×10^{-7}	1.86×10^{-5}	3.89×10^{-5}	3.56×10^{-4}
Differentiability Not Enforced	1.64×10^{-7}	3.20×10^{-6}	1.02×10^{-5}	3.73×10^{-5}
Differentiability Enforced	7.86×10^{-8}	8.86×10^{-7}	5.27×10^{-7}	7.87×10^{-6}

Table 2: Minimum and mean (30 samples) MSE error approximating $y = \sin(x)$ and $y = \tanh(3x)$.

Training Type	Min $\sin(x)$	Min $\tanh(3x)$	Mean $\sin(x)$	Mean $\tanh(3x)$
Default Network	4.50×10^{-5}	5.75×10^{-5}	1.15×10^{-1}	1.96×10^{-1}
RAAI Distribution	3.59×10^{-5}	1.09×10^{-5}	3.63×10^{-2}	2.31×10^{-2}
Pretraining Skipped	1.96×10^{-7}	1.07×10^{-6}	1.93×10^{-5}	8.38×10^{-5}
Differentiability Not Enforced	4.41×10^{-8}	1.49×10^{-7}	1.47×10^{-5}	3.81×10^{-4}
Differentiability Enforced	5.06×10^{-8}	6.82×10^{-8}	2.21×10^{-7}	8.42×10^{-7}

in between them. Enforcing differentiability during pretraining can impart a bias towards smoother solutions during gradient descent and eliminates these occurrences in our experiments.

The last trend to observe is the poor average performance of default networks. In a typical run of these experiments, around half of the default networks collapse. RAAI is able to eliminate most, but not all of the dying ReLU instances due to its probabilistic nature, so it, too, has high mean error.

Our second set of results is shown in Table 3 and in Figure 4. Here the most important impact of utilizing exponentially many linear regions is demonstrated. Not only can more accurate representations of training data be learned, but more linear regions allow the network to better capture underlying nonlinearity to enhance its predictive power in regression tasks. This result is especially significant because it indicates that even in cases where there are fewer data points than linear regions, having the additional regions can still provide performance advantages.

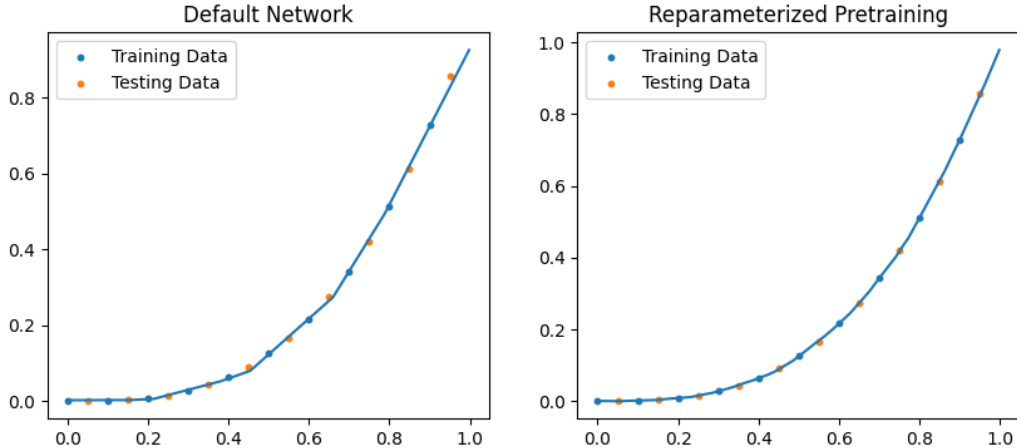


Figure 4: Comparison between standard initialization/gradient descent and pretraining with differentiability enforced. Using more linear regions allows the curve to better predict the test points.

Table 3: Minimum errors on unseen points from training on sparse data.

Training Type	Min x^3	Min x^{11}	Min $\sin(x)$	Min $\tanh(3x)$
Default Network	2.41×10^{-4}	2.14×10^{-3}	2.27×10^{-5}	1.60×10^{-4}
Differentiable Pretraining	5.65×10^{-6}	6.53×10^{-4}	7.92×10^{-7}	5.09×10^{-6}

4.3 Gradient Descent does not Directly Optimize Efficiency

Figure 5 shows the interior of a default network. The layers here are shown before applying ReLU. The default networks fail to make efficient use of ReLU to produce linear regions, even falling short of 1 bend per neuron, which can easily be attained by forming a linear spline (1 hidden layer) that interpolates some of the data points. Examining the figure, the first two layers are wasted. No neuron’s activation pattern crosses $y = 0$, so ReLU is never used. Layer 3 could be formed directly from the input signal. Deeper in the network, more neurons remain either strictly positive or negative. Those that intersect $y = 0$ are monotonic, only able to introduce one bend at a time. The core issue is that while more bends leads to better accuracy, networks that have few bends are not locally connected in parameter space to those that have many. This is problematic since gradients can only carry information about the effects of infinitesimal parameter modifications. If a bend exists, gradient descent can reposition it. But for a neuron that always outputs a strictly positive value (such as the red in layer 2), bends cannot be introduced by infinitesimal weight or bias adjustments. Therefore, bend-related information will be absent from its gradients. Gradient descent will only compel a network to bend by happenstance; indirectly related local factors must guide a neuron to begin outputting negative values. Rarely, these local incentives are totally absent, and the network outputs a bend-free line of best fit.

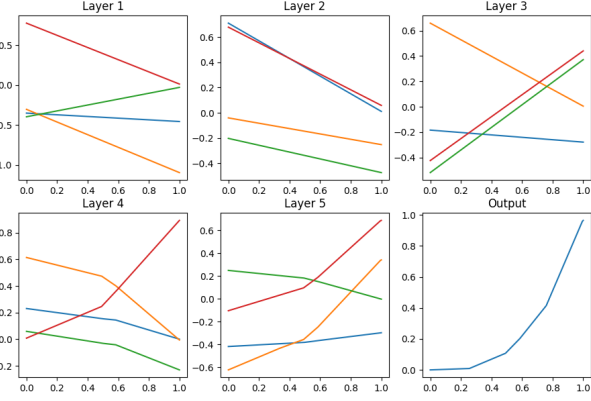


Figure 5: Approximation produced with standard methodologies. The layers are shown before ReLU is applied. The neuron colors here are arbitrary; they do not correspond to Figure 2.

Figure 5 shows the interior of a default network. The layers here are shown before applying ReLU. The default networks fail to make efficient use of ReLU to produce linear regions, even falling short of 1 bend per neuron, which can easily be attained by forming a linear spline (1 hidden layer) that interpolates some of the data points. Examining the figure, the first two layers are wasted. No neuron’s activation pattern crosses $y = 0$, so ReLU is never used. Layer 3 could be formed directly from the input signal. Deeper in the network, more neurons remain either strictly positive or negative. Those that intersect $y = 0$ are monotonic, only able to introduce one bend at a time. The core issue is that while more bends leads to better accuracy, networks that have few bends are not locally connected in parameter space to those that have many. This is problematic since gradients can only carry information about the effects of infinitesimal parameter modifications. If a bend exists, gradient descent can reposition it. But for a neuron that always outputs a strictly positive value (such as the red in layer 2), bends cannot be introduced by infinitesimal weight or bias adjustments. Therefore, bend-related information will be absent from its gradients. Gradient descent will only compel a network to bend by happenstance; indirectly related local factors must guide a neuron to begin outputting negative values. Rarely, these local incentives are totally absent, and the network outputs a bend-free line of best fit.

4.4 Effect of Pretraining on a Compositional Network

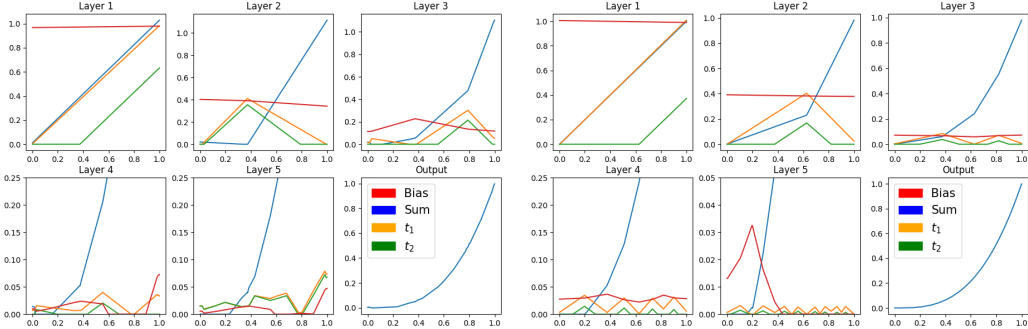


Figure 6: Pretraining (right) results in better structural retention in deeper layers.

In Figure 6 we compare the top performing models with and without reparameterized pretraining. We observe that without the guidance of the pretraining, gradient descent usually loses the triangle

generating structure. It typically happens around layer 4 or 5, devolving into noisy patterns and resulting in higher errors, whereas pretraining maintains structure at greater depths. This behavior of gradient descent we observe is problematic since theoretical works often rely on specific constructions within networks to prove their results. Gradient descent greedily abandons any such structure in favor of models that can be worse in the long term. A theoretical result that shows a certain representation exists in the set of neural networks will thus have a hard time actually learning it without a subsequent plan to control training.

5 Limitations and Extensions

Although our reparameterization can help maintain the triangular structure out to greater depths than unassisted gradient descent, our neurons will still begin producing non-triangular outputs eventually. This suggests that our reparameterization is limited in the functions it can theoretically capture. It may be enabling a rapid error reduction initially in the first few layers, but be unable to approach most curves to arbitrary precision. It is in this remaining error gap that the second stage, gradient descent, becomes lost. In the appendix, we detail two important results concerning the theoretical expressive power of our reparameterization that support this.

First, the differentiability constraints on the scaling parameters during pretraining necessitate that the network outputs a convex function. It is important for the pretraining to be able to produce a reasonably close initial solution; therefore, the reparameterization we use is only guaranteed to be suitable for approximating convex functions. The second limitation we encounter is that pursuing further smoothness (at least in this 4-neuron configuration) is not possible. The appendix show that approximating x^2 is the only way to have a twice continuously differentiable output in the infinite depth limit.

Despite these limitations, these networks could still be considered as replacements of the x^2 gate discussed in Section 2.1. Likewise, they could be used as a base component for assembly into larger networks. These composed networks could learn non-convex functions in higher dimensions, and they would at minimum be guaranteed to represent interpolating polynomials. The drawback is that they would likely become prohibitively large. Rather than approximating another approximation scheme out of ReLU networks, it may be better to focus on finding representations that more naturally arise from ReLU networks themselves when extending this work. Two properties specifically stand out as being somewhat fundamental to deep ReLU approximations: each linear region produced is a full copy of the original input interval $[0, 1]$, and the linear regions' boundaries become dense as depth tends towards infinity. Density ensures that no two inputs are linearly related in an infinite network, and the repeated reproduction of the input space allows each layer to act on each previously existing region independently and simultaneously. These properties both arise in our method, and are likely important considerations when seeking theoretical extensions. Lastly, it might be important to consider non-differentiable model outputs as a way to gain additional flexibility, but additional protections would need to be put in place against overfitting.

6 Concluding Remarks

This paper focused on exploiting the potential computational complexity advantages neural networks offer for the problem of efficiently learning nonlinear functions; in particular, compelling ReLU networks to approximate functions with exponential accuracy as network depth is linearly increased. Our results showed improvements of one to several orders of magnitude in using our reparameterization and pretraining strategy to train ReLU networks to learn various nonlinear, convex, one-dimensional functions. Though further research is required to extend this technique to general multi-dimensional nonlinear functions, the present work's principal significance lies in demonstrating the possibility of converting theoretical ReLU-based constructions into novel training procedures. This finding is particularly powerful since random initialization and gradient descent are not likely to produce an efficient solution on their own, even if it can be proven to exist in the set of sufficiently sized ReLU networks. We are hopeful that future works by our group and others will help illuminate a complete theory for harnessing the potential exponential power of depth in ReLU networks and even more general types of neural networks.

References

Minshuo Chen, Haoming Jiang, Wenjing Liao, and Tuo Zhao. Efficient approximation of deep ReLU networks for functions on low dimensional manifolds. In H. Wallach, H. Larochelle, A. Beygelzimer, F. d'Alché-Buc, E. Fox, and R. Garnett, editors, *Advances in Neural Information Processing Systems*, volume 32. Curran Associates, Inc., 2019. URL https://proceedings.neurips.cc/paper_files/paper/2019/file/fd95ec8df5dbeea25aa8e6c808bad583-Paper.pdf.

Adrian Chmielewski-Anders. Activation regions as a proxy for understanding neural networks. Master's thesis, KTH Royal Institute of Technology, July 2020.

George Cybenko. Approximation by superpositions of a sigmoidal function. *Mathematics of control, signals and systems*, 2(4):303–314, 1989.

I. Daubechies, R. DeVore, S. Foucart, B. Hanin, and G. Petrova. Nonlinear approximation and (deep) ReLU networks. *Constructive Approximation*, 55(1):127–172, Feb 2022. ISSN 1432-0940. doi: 10.1007/s00365-021-09548-z. URL <https://doi.org/10.1007/s00365-021-09548-z>.

Jonathan Frankle and Michael Carbin. The lottery ticket hypothesis: Finding sparse, trainable neural networks, 2019.

Frederic Gibou, David Hyde, and Ron Fedkiw. Sharp interface approaches and deep learning techniques for multiphase flows. *Journal of Computational Physics*, 380:442–463, 2019. doi: 10.1016/j.jcp.2018.05.031. URL <https://doi.org/10.1016/j.jcp.2018.05.031>.

Xavier Glorot and Yoshua Bengio. Understanding the difficulty of training deep feedforward neural networks. In Yee Whye Teh and Mike Titterington, editors, *Proceedings of the Thirteenth International Conference on Artificial Intelligence and Statistics*, volume 9 of *Proceedings of Machine Learning Research*, pages 249–256, Chia Laguna Resort, Sardinia, Italy, 13–15 May 2010. PMLR. URL <https://proceedings.mlr.press/v9/glorot10a.html>.

Boris Hanin. Universal function approximation by deep neural nets with bounded width and ReLU activations. *Mathematics*, 7(10), 2019. ISSN 2227-7390. doi: 10.3390/math7100992. URL <https://www.mdpi.com/2227-7390/7/10/992>.

Boris Hanin and David Rolnick. Deep ReLU networks have surprisingly few activation patterns. In H. Wallach, H. Larochelle, A. Beygelzimer, F. d'Alché-Buc, E. Fox, and R. Garnett, editors, *Advances in Neural Information Processing Systems*, volume 32. Curran Associates, Inc., 2019. URL https://proceedings.neurips.cc/paper_files/paper/2019/file/9766527f2b5d3e95d4a733fcfb77bd7e-Paper.pdf.

Kaiming He, Xiangyu Zhang, Shaoqing Ren, and Jian Sun. Delving deep into rectifiers: Surpassing human-level performance on imagenet classification. In *Proceedings of the IEEE International Conference on Computer Vision (ICCV)*, December 2015.

Kurt Hornik, Maxwell Stinchcombe, and Halbert White. Multilayer feedforward networks are universal approximators. *Neural Networks*, 2(5):359–366, 1989. ISSN 0893-6080. doi: [https://doi.org/10.1016/0893-6080\(89\)90020-8](https://doi.org/10.1016/0893-6080(89)90020-8). URL <https://www.sciencedirect.com/science/article/pii/0893608089900208>.

Irena Ivanova and Miroslav Kubat. Initialization of neural networks by means of decision trees. *Knowledge-Based Systems*, 8(6):333–344, 1995.

Diederik P. Kingma and Jimmy Ba. Adam: A method for stochastic optimization, 2017.

Shiyu Liang and R. Srikant. Why deep neural networks? *CoRR*, abs/1610.04161, 2016. URL <http://arxiv.org/abs/1610.04161>.

Jianfeng Lu, Zuowei Shen, Haizhao Yang, and Shijun Zhang. Deep network approximation for smooth functions. *SIAM Journal on Mathematical Analysis*, 53(5):5465–5506, jan 2021. doi: 10.1137/20m134695x. URL <https://doi.org/10.1137/20m134695x>.

Lu Lu, Yeonjong Shin, Yanhui Su, and George Em Karniadakis. Dying ReLU and initialization: Theory and numerical examples. *Communications in Computational Physics*, 28(5):1671–1706, 2020. ISSN 1991-7120. doi: <https://doi.org/10.4208/cicp.OA-2020-0165>. URL http://global-sci.org/intro/article_detail/cicp/18393.html.

Zhou Lu, Hongming Pu, Feicheng Wang, Zhiqiang Hu, and Liwei Wang. The expressive power of neural networks: A view from the width. In I. Guyon, U. Von Luxburg, S. Bengio, H. Wallach, R. Fergus, S. Vishwanathan, and R. Garnett, editors, *Advances in Neural Information Processing Systems*, volume 30. Curran Associates, Inc., 2017. URL https://proceedings.neurips.cc/paper_files/paper/2017/file/32cbf687880eb1674a07bf717761dd3a-Paper.pdf.

Hadrien Montanelli, Haizhao Yang, and Qiang Du. Deep ReLU networks overcome the curse of dimensionality for bandlimited functions, 2020.

Sayan Nag, Mayukh Bhattacharyya, Anuraag Mukherjee, and Rohit Kundu. Serf: Towards better training of deep neural networks using log-softplus error activation function. In *Proceedings of the IEEE/CVF Winter Conference on Applications of Computer Vision (WACV)*, pages 5324–5333, January 2023.

Dmytro Perekrestenko, Philipp Grohs, Dennis Elbrächter, and Helmut Bölcskei. The universal approximation power of finite-width deep relu networks, 2018.

Xuan Qi, Yi Wei, Xue Mei, Ryad Chellali, and Shipin Yang. Comparative analysis of the linear regions in ReLU and LeakyReLU networks. In Biao Luo, Long Cheng, Zheng-Guang Wu, Hongyi Li, and Chaojie Li, editors, *Neural Information Processing*, pages 528–539, Singapore, 2024. Springer Nature Singapore. ISBN 978-981-99-8132-8.

Yeonjong Shin and George Em Karniadakis. Trainability of ReLU networks and data-dependent initialization. *Journal of Machine Learning for Modeling and Computing*, 1(1):39–74, 2020. ISSN 2689-3967.

Dayal Singh and G J Sreejith. Initializing ReLU networks in an expressive subspace of weights, 2021.

Matus Telgarsky. Representation benefits of deep feedforward networks, 2015.

Qingcan Wang et al. Exponential convergence of the deep neural network approximation for analytic functions. *arXiv preprint arXiv:1807.00297*, 2018.

Dmitry Yarotsky. Error bounds for approximations with deep ReLU networks. *Neural Networks*, 94:103–114, 2017. ISSN 0893-6080. doi: <https://doi.org/10.1016/j.neunet.2017.07.002>. URL <https://www.sciencedirect.com/science/article/pii/S0893608017301545>.

7 Appendix

7.1 Training Algorithm

Given a vector $A = [a_0, a_1, \dots, a_n]^T$ the input, output and hidden ($i \in (0, n-1)$) layers of a compositional network will be set as follows:

$$I(x) = \begin{bmatrix} x \\ x \\ x \\ 0 \end{bmatrix} + \begin{bmatrix} 0 \\ 0 \\ -a_0 \\ 1 \end{bmatrix}$$

$$H_i(x) = \begin{bmatrix} 1 & S_i/a_i & -S_i/(a_i - a_i^2) & 0 \\ 0 & S_i/a_i & -S_i/(a_i - a_i^2) & 0 \\ 0 & S_i/a_i & -S_i/(a_i - a_i^2) & -S_i a_{i+1} \\ 0 & 0 & 0 & S_i \end{bmatrix} \times \text{ReLU}(H_{i-1}(x))$$

$$O(x) = [1 \quad S_n/a_n \quad -S_n/(a_n - a_n^2) \quad 0] \times \text{ReLU}(H_{n-1}(x))$$

where S_i can either be chosen independently, or chosen based on A . In the latter case, Equation (4) gives $S_i = s_i/s_{i-1} = (1 - a_i)a_{i+1}$. This initialization process is used in each iteration of the pretraining algorithm.

Algorithm 1 Pretraining

```

 $A \leftarrow \text{Random}((0, 1)^n)$ 
while Epochs > 0 do
    Network  $\leftarrow \text{Initialize}(A)$  ▷ Set weights as above each iteration
    Loss  $\leftarrow (\text{Network}(x) - y)^2$ 
    Network-Gradient  $\leftarrow \text{Derivative}(\text{Loss}, \text{Network})$  ▷ Regular Backpropagation
    A-Gradient  $\leftarrow \text{Derivative}(\text{Network}, A)$  ▷ Backpropagate through Initialization
    Gradient  $\leftarrow \text{Network-Gradient} \times \text{A-Gradient}$ 
     $A \leftarrow A - \epsilon \times \text{Gradient}$  ▷ Update A, Not the network
end while

```

The network can then be initialized once more on the learned vector A so that the network weights can be updated via regular gradient descent. In our experiments both phases of training ran for 1000 epochs

7.2 Derivations

For convenience we first restate the functions defined in the main body of the paper.

$$T_i(x) = \begin{cases} \frac{x}{a_i} & 0 \leq x \leq a_i \\ 1 - \frac{x-a_i}{1-a_i} & a_i \leq x \leq 1 \end{cases}$$

$$T'_i(x) = \begin{cases} \frac{1}{a_i} & 0 < x < a_i \\ \frac{-1}{1-a_i} & a_i < x < 1 \end{cases}$$

$$W_i(x) = \bigcirc_{j=0}^i T_j(x) = T_i(T_{i-1}(\dots T_0(x)))$$

$$F(x) = \sum_{i=0}^{\infty} s_i W_i(x)$$

Notationally, we will denote the sorted x -locations of the peaks and valleys of $W_i(x)$ by the lists $P_i = \{x : W_i(x) = 1\}$ and $V_i = \{x : W_i(x) = 0\}$. We will use the list B_i to reference the locations of all non-differentiable points, which we refer to as bends. $B_i := P_i \cup V_i$. $f_i(x) = \sum_{n=0}^{i-1} s_n W_n(x)$ will denote finite depth approximations up to but not including layer i . The error function $E_i(x) = \sum_{n=i}^{\infty} s_n W_n(x) = F(x) - f_i(x)$ will represent the error between the finite approximation and the infinite depth network.

The goal of this section will be to show how to select the s_i based on a_i in a manner where the derivative $F'(x)$ is defined on all of $[0, 1]$. Fortunately, the left and right derivative limits $F'_+(x)$ and $F'_{-}(x)$ already exist, since each bend in each W_i will use the slope of the line segment to its left or right respectively. The problem is that without choosing the scaling parameters appropriately, $F'_+(x)$ and $F'_{-}(x)$ will take different values so that $F'(x)$ will be undefined on all bend points.

Figure 7 highlights some important properties about composing triangle functions. Peaks alternate with valleys. Peak locations in one layer become valleys in the next. Valleys in one layer remain valleys in all future layers since 0 is a fixed point of each T_i . To produce W_i , each line segment of W_{i-1} becomes a dilated copy of T_i . Each triangle function has two distinct slopes $1/a_i$ and $-1/(1-a_i)$

which are dilated by the chain rule during the composition. On negative slopes of W_{i-1} , the input to layer i is reversed, so those copies of T_i are reflected. Due to the reflection, the slopes of W_i on each side of a peak or valley are proportional. Alternatively, one could consider that on each side of a peak in W_{i-1} , there is a neighborhood of points that are greater than a_i , and are composed with the same line segment of T_i that has slope $-1/(1-a_i)$. Either way, it's important to note that the slopes on each side of a bend scale identically during each composition.

Before we begin reasoning about $F'(x)$, it can simplify the analysis to only consider the derivative of the error function $E'(x)$.

Lemma 7.1. *for $x \in P_i$, $F'(x)$ is defined if and only if $E'_i(x)$ is defined.*

Proof. All of $W_n(x)$ for $n < i$ are differentiable at $x \in P_i$ since x will lie in the interior of a linear region of W_n . Therefore, $f'_i(x) = \sum_{n=0}^{i-1} s_n W'_n(x)$ exists at these points. Since $E'_i + f'_i = F'$, $F'(x)$ is defined if and only if $E'_i(x)$ is defined. \square

Here we compute the right derivative $(E_i)'_+(x)$ of the error function at a point x . The left derivative will only be different by a constant factor.

Lemma 7.2. *For all $x \in P_i$, $E'_+(x)$ and $E'_{-}(x)$ are proportional to*

$$s_i - \frac{1}{1-a_{i+1}} \left(s_{i+1} + \sum_{n=i+2}^{\infty} s_n \prod_{k=i+2}^n \frac{1}{a_k} \right). \quad (5)$$

Proof. Let x_n be some point in P_i , and let n be its index in any list it appears in. To calculate the value of $E'_+(x) = \sum_{n=i}^{\infty} s_n (W_n)'_+(x)$, we will have to find the slope of the linear intervals to the immediate

right of x_n for all W_i . The terms in the summation (5) mostly derive from the chain rule. We will use R to represent $W'_{i+}(x)$. The first term in the sum will be $R s_i \cdot W'_{i+1}(x) = T'_{i+1}(W_i(x))W'_i(x)$ since the derivatives of composed functions will multiply. There are two different possible slope values of T_{i+1} to multiply by, and the correct one to multiply is $-1/(1-a_{i+1})$ because x_n is a peak of W_i , so $W_i(x) > a_{i+1}$ for $x \in (B_{i+1}[n-1], B_{i+1}[n+1])$. This gives $W'_{i+1}(x) = -R \frac{s_{i+1}}{(1-a_{i+1})}$. Note that the second term has the opposite sign as the first.

For all remaining terms, since x_n was in P_i , it is in V_j for $j > i$. For $x \in (B_{j+1}[n-1], B_{j+1}[n+1])$, $W_j(x) < a_{j+1}$ and the chain rule applies the first slope $1/a_{j+1}$. Since this slope is positive, every term has the opposite sign as the first. Summing up all the terms with the coefficients s_i , and factoring out R will yield the desired formula. Note that this same reasoning applies to the left side, the initial slope L will just be different. \square

Lemma 7.3. *If $E'_+(x) = E'_-(x)$, $E'(x)$ must be equal to 0.*

Proof. Let S represent Equation (5), and R and L be the constants of proportionality for the directional derivatives. If $E'_+ = E'_-$, then $R_x S = L_x S$ for all $x \in P_i$. Since W_i is comprised of alternating positive and negatively sloped line segments, R_x and L_x have opposite signs. The only way to satisfy the equation then is if $S = 0$. Consequently, $E'(x) = 0$ for all $x \in P_i$. \square

This lemma shows that to calculate the derivative at of $F(x)$ for any bend point x (whenever it's actually defined), one needs only to compute the derivative of the finite approximation f_i (which excludes W_i). This will be useful later for proving other results. A visualization of this lemma is provided in Figure 8

Lemma 7.4. *For all $x \in P_i$:*

$$F'(x) = f'_i(x) = \sum_{j=0}^{i-1} s_j W'_j(x) \quad (6)$$

Proof. From the previous lemma we have $E'(x) = 0$ whenever the directional derivatives are equal. $F(x) = \sum_{j=0}^{i-1} s_j W_j(x) + E(x)$. The first $i-1$ terms are differentiable at the points P_i since those points lie between the discontinuities in B_{i-1} . Therefore $F'(x)$ is defined and can be calculated using the finite sum. \square

We now prove our main theorem. Intuitively, the theorem shows that there is a way to sum the triangular waveforms W_i so that the resulting function approximation converges to a differentiable function, which, as mentioned at the start of this subsection, can aid in preventing overfitting when using exponentially many linear regions. The idea of the proof is that much of the formula for $E'(x)$ will be shared between two successive generations of peaks. Once they are both valleys, they will behave the same, so the sizes of their remaining discontinuities will need to be proportional.

Theorem (3.1). *$F'(x)$ is defined on $[0, 1]$ only if the scaling coefficients are selected based on a_i according to:*

$$s_{i+1} = s_i(1 - a_{i+1})a_{i+2}$$

Proof. Rewriting Equation (5) (which is equal to 0) for layers i and $i+1$ in the following way:

$$\begin{aligned} s_i(1 - a_{i+1}) &= s_{i+1} + \frac{1}{a_{i+2}} \left(s_{i+2} + \sum_{n=i+3}^{\infty} s_n \prod_{k=i+3}^n \frac{1}{a_k} \right) \\ s_{i+1}(1 - a_{i+2}) &= s_{i+2} + \sum_{n=i+3}^{\infty} s_n \prod_{k=i+3}^n \frac{1}{a_k} \end{aligned}$$

allows for a substitution to eliminate the infinite sum

$$s_i(1 - a_{i+1}) = s_{i+1} + \frac{1 - a_{i+2}}{a_{i+2}} s_{i+1}$$

Collecting all the terms gives

$$s_{i+1} = \frac{s_i(1 - a_{i+1})}{1 + \frac{1 - a_{i+2}}{a_{i+2}}}$$

which simplifies to the desired result. \square

7.3 Sufficiency for differentiability

We can show that in addition to being necessary for the existence of the derivative on the bend points, our choice of scaling is sufficient when a_i are bounded away from 0 or 1.

Theorem 7.5. $F'(x)$ is well-defined if we can find $c > 0$ such that $c \leq a_i \leq 1 - c$ for all i and choose all s_i according to Equation (4).

Proof. We begin by considering Equation (5) for layer i (it equals 0 by Theorem (7.3)).

$$s_i = \frac{1}{1 - a_{i+1}} \left(s_{i+1} + \sum_{n=i+2}^{\infty} s_n \prod_{k=i+2}^n \frac{1}{a_k} \right)$$

We will prove our result by substituting Equation (4) into this formula, and then verifying that the resulting equation is valid. First we would like to rewrite each s_n in terms of s_i . Equation (4) gives a recurrence relation. Converting it to a non-recursive representation we have:

$$s_n = s_i \left(\prod_{j=i+1}^n 1 - a_j \right) \left(\prod_{k=i+2}^{n+1} a_k \right) \quad (7)$$

When we substitute this into Equation (5), three things happen: each term is divisible by s_i so s_i cancels out, every factor in the product except the last cancels, and $1 - a_{i+1}$ cancels. This leaves

$$1 = a_{i+2} + (1 - a_{i+2})a_{i+3} + (1 - a_{i+2})(1 - a_{i+3})a_{i+4} + \dots = \sum_{n=i+2}^{\infty} a_n \prod_{m=i+2}^{n-1} (1 - a_m) \quad (8)$$

This equation has an interpretation that is important to the argument. 1 represents the full size of the initial discontinuity at a point in P_i , and each term on the other side represents how much the discontinuity is closed for each triangle wave that is added. Every time a wave is added, it can be thought of as subtracting from each side the first term appearing on the right. We will now show that each term of the sum on the right accounts for a fraction (equal to a_i) of the remaining error. Inductively we can show:

$$1 - \sum_{n=i+2}^j a_n \prod_{m=i+2}^{n-1} (1 - a_m) = \prod_{m=i+2}^j (1 - a_m) \quad (9)$$

This means that as the first term appearing on the right is repeatedly subtracted, that term is always equal to a_n times the left side. As a base case, we have $(1 - a_{i+2}) = (1 - a_{i+2})$. Assuming the above equation holds for all previous values of j

$$1 - \sum_{n=i+2}^{j+1} a_n \prod_{m=i+2}^{n-1} (1 - a_m) = 1 - \sum_{n=i+2}^j a_n \prod_{m=i+2}^{n-1} (1 - a_m) - a_{j+1} \prod_{m=i+2}^j (1 - a_m) =$$

using the inductive hypothesis to make the substitution

$$\prod_{m=i+2}^j (1 - a_m) - a_{j+1} \prod_{m=i+2}^j (1 - a_m) = \prod_{m=i+2}^{j+1} (1 - a_m)$$

Since all $c < a_i < 1 - c$, the size of the discontinuity at the points P_i is upper bounded by the exponentially decaying series $(1 - c)^n$, which approaches zero. \square

7.4 Error Decay

Lemma 7.6. *The ratio s_{i+2}/s_i is at most 0.25.*

Proof. by applying Equation (4) twice, we have

$$s_{i+2} = s_i(1 - a_{i+1})(1 - a_i + 2)a_{i+2}a_{i+3}$$

To maximize s_{i+2} we choose $a_{i+1} = 0$ and $a_{i+3} = 1$. The quantity $a_{i+2} - a_{i+2}^2$ is a parabola with a maximum of 0.25 at $a_{i+2} = 0.5$. \square

Since each W_i takes values between 0 and 1, its contribution to F is bounded by s_i . Since the s_i decay exponentially, one could construct a geometric series to bound the error of the approximation and arrive at an exponential rate of decay.

7.5 Second Derivatives

Here we show that any function represented by one of these networks that is not $y = x^2$ does not have a second derivative defined at the bend locations. To show this we will sample a discrete series of $\Delta y/\Delta x$ values from $F'(x)$ and show that the limits of these series on the right and left are not the same (unless all $a_i = 0.5$), which implies that $F''(x)$ does not exist (see Figure 8 below). First we will produce the series of Δx . Let x be the location of a peak of W_i , and let l_n and r_n be its immediate neighbors in B_{i+n} .

Lemma 7.7. *If $c < a_i < 1 - c$ for all i , we have $\lim_{n \rightarrow \infty} r_n = \lim_{n \rightarrow \infty} l_n = x$. Furthermore, $r_n, l_n \neq x$ for any finite i .*

Proof. Let R and L denote the magnitude of W'_i on the left and right of x . x is a peak location of W_i , so the right side slope is negative and the left is positive. Solving for the location of $T_{i+1}(W_i(x)) = 1$ on each side will give $l_1 = x - (1 - a_{i+1})/L$ and $r_1 = x + (1 - a_{i+1})/R$.

On each subsequent iteration $i + n$ ($n \geq 2$), x is a valley point and the Δx intervals get multiplied by a_{i+n} . Since x is a valley point the right slope is positive and the left is negative. The slope magnitudes are given by $\frac{1}{x - l_n}$ and $\frac{1}{r_n - x}$ since W_{i+n} ranges from 0 to 1 over these spans. Solving for the new peaks again will give $l_{n+1} = x - a_{i+1}(x - l_n)$ and $r_{n+1} = x + a_{i+1}(r_n - x)$. The resulting non-recursive formulas are:

$$x - l_n = \frac{1 - a_{i+1}}{L} \prod_{m=2}^n a_{i+m} \text{ and } r_n - x = \frac{1 - a_{i+1}}{R} \prod_{m=2}^n a_{i+m} \quad (10)$$

The right hand sides will never be equal to zero with a finite number of terms since a parameters are bounded away from 0 and 1 by c . \square

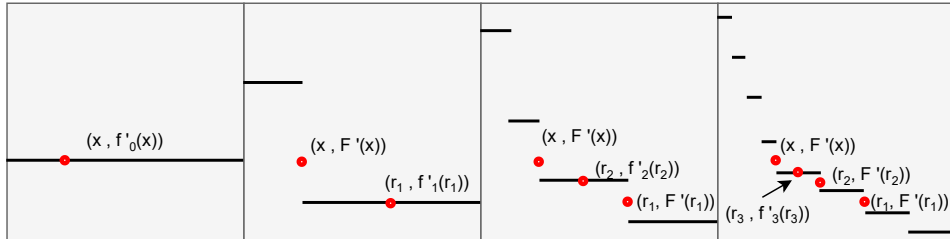


Figure 8: The derivatives of the first few stages of approximation. Notice that each time a constant segment "splits", the two neighboring segments adjacent to the split converge back to the original value. The points in the series approaching x from the right are marked. $a_0 \neq 0.5$ and all other parameters are set to 0.5, which will cause the left and right sets of points to lie on lines with different slopes.

Next we derive the values of Δy to complete the proof.

Theorem 7.8. $F(x)$ cannot be twice differentiable unless $F(x) = x^2$.

Proof. The points l_n and r_n are all peak locations, Equation (6) gives their derivative values as $f'_{i+n}(r_n)$. In our argument for sufficiency, we reasoned about the sizes of the discontinuities in f' at x . Since l_n and r_n always lie on the linear intervals surrounding x as $n \rightarrow \infty$, we can get the value of $f'_i(x) - f'_{i+n}(r_n)$ using Equation (9) with the initial discontinuity size set to $R * s_i$ rather than 1. Focusing on the right hand side we get:

$$f'_i(x) - f'_{i+n}(r_n) = R * s_i \prod_{m=2}^n (1 - a_{i+m})$$

taking $\Delta y / \Delta x$ gives a series:

$$\frac{R^2 s_i}{(1 - a_{i+1})} \prod_{m=i+2}^n \frac{1 - a_m}{a_m}$$

The issue which arises is that the derivation on the left is identical, except for a replacement of R by L . The only way for these formulas to agree then is for $R = L$ which implies $a_i = 1 - a_i = 0.5$. Since this argument applies at any layer, then all a parameters must be 0.5 (which approximates $y = x^2$). \square

7.6 Convexity

Each of the f'_i are composed of constant value segments, we will show that those values are monotonically decreasing (this can be seen in Figure8). This then allows us to show that F is convex.

Lemma 7.9. The function $F(x)$ is convex when all s_i are chosen according to Equation (4).

Proof. To establish this we will introduce the list $Y'_i = [F'(V_i[0]), f'_i(V_i[n]), F'(V_{i+1}[2^i])]$ for $0 \leq n \leq 2^i$, which tracks the values of F' at the i^{th} set of valley points. All but the first and last points will have been peaks at some point in their history, so Equation (6) gives the value of those derivatives as f'_i .

We establish two inductive invariants. One is that the y-values in the list Y_i remain sorted in descending order. The other is that $Y'_i[n] \geq f'_i(x) \geq Y'_i[n+1]$ for $V_i[n] < x < V_i[n+1]$, indicating that the constant value segments of f'_i lie in between the limits in the list Y_i . Together, these two facts imply that each iteration of the approximation f_i is convex. Which then implies that their limit F is also convex.

As the base case f_0 is a line with derivative 0, V_0 contains its two endpoints. Y'_0 is positive for the left endpoint (negative for right) since on the far edges F' is a sum of a series of positive (or negative) slopes, Therefore both the points in Y' are in descending sorted order. The second part of the invariant is true since 0 is in between those values.

Consider an arbitrary interval $(V_i[n], V_i[n+1])$ of f_i , this entire interval is between two valley points, so f'_i (which hasn't added W_i yet) is some constant value, which we know from the second inductive hypothesis is in between $Y'_i[n]$ and $Y'_i[n+1]$. The point $x \in P_i \cap (V_i[n], V_i[n+1])$ will have $F'(x) = f'_i(x)$, and it will become a member of V_{i+1} . This means we will have $Y_{i+1}[2n] > Y_{i+1}[2n+1] > Y_{i+1}[2n+2]$, maintaining sorted order of Y' .

Adding $s_i W_i$ takes f_i to $f_i + 1$ splitting each constant valued interval in two about the points P_i , increasing the left side, and decreasing the right side. Recalling from the derivation of Equation (5) all terms but the first in the sum have the same sign, so the limiting values in Y'_i are approached monotonically. Using the first inductive hypothesis, we have on the left interval $Y'_i[n] = Y'_{i+1}[2n] > f'_{i+1} > f'_i = Y'_{i+1}[2n+1]$ and on the right we have $f'_i = Y'_{i+1}[2n+1] > f_{i+1} > Y'_i[n+1] = Y'_i[2n+2]$. And so each constant interval f_{i+1} remains bounded by the limits in Y'_{i+1} .

We will now show by contradiction that the limit F of the sequence of f_i is convex. Assume that F is non-convex. Then there exists points a , b , and c such that $F(b)$ lies strictly below the line connecting the points $(a, F(a))$ and $(c, F(c))$. Lets say it's below the line by an amount ϵ . Since at each point f_i converges to F , we can find i_a such that $f_{i_a}(a) - F(a) < \epsilon/2$, etc..., we take $i = \max(i_a, i_b, i_c)$. Since the line connecting $(a, f_i(a))$ and $(c, f_i(c))$ is no more than $\epsilon/2$ lower, and $f_i(c)$ no more than $\epsilon/2$ higher, $f_i(c)$ must still lie below the line, making f_i non-convex and producing a contradiction. \square

Potential Broader Impact

This paper presents work whose goal is to enable more efficient neural networks. While the present work is largely theoretical, future advances in this line of research could enable the use of much smaller networks in many practical applications, which could substantially mitigate the rapidly growing issue of energy usage in large learning systems.